Yield Limits of Plates at Extremely High Heat Flux

John H. Lienhard V
Dominic S. Napolitano

W. M. Rohsenow Heat and Mass Transfer Laboratory
Department of Mechanical Engineering, Room 3-162
Massachusetts Institute of Technology
Cambridge, MA 02139-4307

Abstract

For heat fluxes ranging above 10 MW/m^2 or so, solid surfaces usually experience large thermal stresses and degradation of mechanical properties. The resulting mechanical failure of such surfaces is a primary limitation to the design of thermal systems at extremely high heat flux. This investigation considers the elastic stresses in circular plates subjected to extremely high heat fluxes. A gaussian distributed heat load is applied to one surface of the plate and the heat flux at which yielding occurs is identified. Several candidate materials are examined, accounting for the temperature dependence of yield strength and other properties. The mechanical boundary conditions on the plate are varied. Figures of merit are given for the high flux performance of a number of materials.

Journal of Heat Transfer, Vol. 120, February 1998

Nomenclature

Roman Letters

a	gaussian decay rate (see Eq. (2); m)
b	plate radius (m)
E	Young's modulus (N/m^2)
$F(r)$	see Eq. (7)
H	thickness of plate (m)
k	thermal conductivity (W/m·K)
M_r, M_θ	bending moment in the r, θ direction per unit length (N)
N_r, N_θ	membrane force in the r, θ direction per unit length (N/m)
q	heat flux (W/m^2)
Q_{efm}	material figure of merit for elastic deformation (MW·mm/m^2)
(r, z, θ)	cylindrical coordinates
T	temperature distribution (K)
$\overline{T}(r)$	mean temperature over plate thickness (see Eq. (3); K)
T_c	low temperature at top of plate (K)
T_h	high temperature at bottom of plate (see Eq. (2); K)
T_{melt}	melting or solidus temperature of material (K)
T_0	temperature of plate in unstressed initial state (K)

Greek Letters

α	thermal expansion coefficient (K^{-1})
$\Delta T(r)$	temperature difference across plate thickness (see Eq. (3); K)
ν	Poisson's ratio
σ_{jj}	normal stress in the j-direction (N/m^2)
σ_v	von Mises stress (N/m^2)
σ_Y	0.2% yield stress (N/m^2)

1 Introduction

The creation of steady heat fluxes on the order of 100 MW/m^2 through solids is usually hampered by mechanical failure of the heat transfer surface, resulting from thermal stress and loss of material strength. Unique features of thermal stress management at extremely high heat fluxes include temperatures that may approach the melting point of the solid surface and temperature differences of more than 1000°C imposed over distances of only a few millimeters. Yield strength may become very low on the hot side of the solid, leading to plastic deformation or rupture.

For a solid of a given thickness, the highest one-dimensional heat flux that may be sustained places one surface at the melting point while the opposite surface is held at low temperature (typically the temperature of a coolant, such as water near 25°C). Conditions of this sort have produced the highest steady state heat fluxes to be obtained. In particular, Liu and Lienhard (1993) achieved fluxes of up to 400 MW/m^2 through a molybdenum plate cooled by a high speed water jet on one side and heated to its melting point by a plasma arc struck to its opposite side; in this state, the unmelted thickness of the molybdenum sheet was less than 1 millimeter. Tests run on other materials of similar thermal conductivity showed failures at lower heat fluxes, typically by plastic rupture or brittle fracture. All evidence suggested that failure was a function of the solid material used and did not derive from limitations of the cooling process (such as a critical heat flux phenomenon). Thermal stresses were the apparent cause of these failures.

Simple one-dimensional thermal stress calculations show that stresses in a plate subjected to the melting point flux can easily exceed the elastic strength, and finite-element simulations allowing for plasticity show that the stresses may exceed ultimate strength (Lienhard and Napolitano, 1996). The stress levels actually achieved depend on the specific material used, the mechanical boundary conditions of the plate, and the temperature difference developed across the plate for a given heat flux.

This paper identifies the flux at which thermal stress reaches yield strength for several promising materials in a configuration generically similar to that found in some of the highest heat flux systems. Our focus is on planar surfaces that are heated from one face and cooled from the opposite face; this geometry is typical of various extremely high flux systems, notably those involving jet impingement cooling. Heat loads are taken to be gaussian distributed on the hot surface, as is typical of the optical beam heating or plasma-arc heating that is frequently used to reach the highest fluxes. Our objective is to sort out the influence of several factors affecting the mechanical performance of extremely high flux systems. These factors include material properties, heat load distributions, and mechanical constraints. The onset of yielding is taken as a measure of material performance; other important issues, such as creep and thermal fatigue, are not considered.

We assume steady-state in analyzing the stresses. Transient stresses can be larger

in systems that experience an abrupt change in boundary temperature, owing to the highly nonlinear temperature distributions that may occur during transients. However, current extremely high heat flux systems most often involve applied heat fluxes (*e.g.*, laser beams), and for those cases the maximum stress may occur in either the steady or transient state depending on the heating profile and the mechanical boundary condition. We assume our steady states to be reached through a quasisteady heating process in which the temperature distribution through the plate thickness is always linear.

2 Materials for High Heat Fluxes

Materials for use at extremely high heat fluxes must have a combination of high thermal conductivity, high strength at elevated temperature, low thermal expansion, and/or low elastic modulus. In this paper, we consider some typical metals, either high conductivity metals (copper and aluminum) or refractory metals (tungsten and molybdenum). A cold-worked stainless steel is examined for comparison. Yield strengths of these materials are shown in Figure 1 and properties of these and other materials are listed in Table 1 (Touloukian, 1979; Holt et al., 1995; Peckner and Bernstein, 1977; ASM, 1985).

Fig. 1

Table 1

Precipitation-hardening coppers, such as chromium copper (C18200) and zirconium copper (C15000), are useful owing to their high strength after cold-working and aging. This strength is retained for temperatures up to a few hundred Celsius. Dispersion-strengthed coppers, such as C15715, obtain strength from aluminum oxide powder dispersed in the copper matrix. These coppers have thermal and elastic properties nearly identical to aged-hardened coppers, but they soften less at high temperatures and exhibit much better creep/rupture characteristics. Aluminum alloys do not retain their strength beyond about 150°C. The coppers and aluminums in the table are hardened to the tempers indicated.

Refractory metals have reasonably high thermal conductivities and can retain cold working at high temperatures (recrystallization above 900°C for molybdenum and 1300°C for tungsten). Some refractory metals will have ductile-to-brittle transition temperatures in the operating temperature range (DTBT around 200°C for tungsten, near room temperature for molybdenum, but near absolute zero for tantalum). Most refractories require protection from oxidation at high temperatures. The molybdenum alloy TZM (Mo-0.5Ti-0.1Zr) has higher strength than pure molybdenum, a higher recrystallization temperature, and better creep characteristics.

Stainless steels and superalloys have low thermal conductivity and are usually unsuitable for extremely high heat flux applications. To illustrate this, 304L stainless steel with 10% cold reduction is examined in some the following sections. Other materials of interest for high heat fluxes include synthetic diamond (see Table 1) and ceramics such as silicon carbide.

Previous studies (Abdou et al., 1984; Lienhard and Khounsary, 1993) have proposed

the following figure of merit for the elastic performance of high heat flux materials:

$$Q_{\text{efm}} \equiv \frac{(1-\nu)k\sigma_Y}{E\alpha}. \tag{1}$$

This figure is effectively based on the thermal stress in a uniformly heated, fixed-edge plate; it represents the flux that causes yield stress in a plate of unit thickness. Values are listed in Table 1 for various materials. This figure of merit gives a reasonable first-order approximation to the performance of a particular material, but for some materials it decreases sharply as temperature rises owing to the temperature dependence of yield strength. Moreover, stresses can be lower for plates that have only localized heating or for plates that are allowed to expand laterally. Consequently, a more complete analytical ranking of materials is desirable.

3 Localized Heating of an Axisymmetric Disk

We consider a steady localized heat source applied to one side of a circular disk and compute the heat flux at which yielding first occurs within the disk. Our objective is to identify major factors affecting stresses during localized heating and to estimate the heat fluxes achievable without plastic deformation.

Fig. 2

A circular plate of radius b and thickness H is considered (Figure 2). Cylindrical coordinates (r, z, θ) are located at the plate center with the z-axis directed upward. Calculations are based on classical plate theory. The plate's material properties, other than yield stress, are treated as homogeneous and temperature independent; yield stress is evaluated at the local temperature to determine the elastic limit. Comparison to finite element simulations with fully variable properties shows that the present property approximation is accurate to within 10 to 15% if properties other than yield strength are evaluated at the average temperature of the plate (Dahbura, 1996).

A gaussian distributed temperature profile is assumed; as previously noted, such temperature profiles are typical of localized heating by optical beams or plasma arcs. The plate is unstressed at a temperature of $T_0 = 25°\text{C}$. The imposed temperature distribution on the *bottom* surface of the plate ($z = -H/2$) is an axisymmetric Gaussian profile

$$T_h(r) = T_c + \left(T_{\max} - T_c\right) \exp\left(-\frac{2r^2}{a^2}\right) \tag{2}$$

and the upper surface is held (as by intense convective cooling) to $T_c = T_0$. The gaussian temperature distribution is assumed to decay slowly enough with radius that the temperature variation in z for fixed r is essentially a linear variation between the upper and lower surface temperatures.[1] The temperature field in the plate is thus

$$T(r,z) \quad = \quad \left(\frac{T_h(r) + T_c}{2}\right) + \left(\frac{z}{H}\right)\left(T_h(r) - T_c\right)$$

[1] This condition is satisfied when radial heat conduction is negligible, *i.e.*, for $(H/a)^2 \ll 1$.

$$\equiv \quad T_0 + \overline{T}(r) - \left(\frac{z}{H}\right)\Delta T(r). \tag{3}$$

The stresses in the plate can be calculated by integration of standard equations from classical plate theory (Johns, 1965; Tauchert, 1986; Boley and Weiner, 1960). Plate theory leads to general expressions for the membrane forces per unit length, N_r and N_θ, and for the bending moments per unit length, M_r and M_θ; for brevity, we omit the general equations, which are well known. The moments and forces must be calculated for our particular temperature field; then, the stresses resulting from a temperature field of the form (3) may be calculated as follows.

$$\sigma_{rr} = \frac{N_r}{H} + \left(\frac{12z}{H^3}\right) M_r \tag{4}$$

$$\sigma_{\theta\theta} = \frac{N_\theta}{H} + \left(\frac{12z}{H^3}\right) M_\theta \tag{5}$$

3.1 Simply Supported Plate

In this case, the edge of the plate has zero vertical deflection and zero radial stress or bending moment. The solutions for the bending moments on the interior are (Johns, 1965)

$$M_r = \frac{EH^2}{12}\left(\frac{1}{r^2}F(r) - \frac{1}{b^2}F(b)\right) \tag{6}$$

$$M_\theta = \frac{EH^2}{12}\left(\alpha\Delta T(r) - \frac{1}{r^2}F(r) - \frac{1}{b^2}F(b)\right)$$

where

$$F(r) = \int_0^r r\alpha\Delta T(r)\,dr \tag{7}$$

and the membrane forces are

$$N_r = \frac{E\alpha H}{r^2}\left(\frac{r^2}{b^2}\int_0^b r\overline{T}(r)\,dr - \int_0^r r\overline{T}(r)\,dr\right) \tag{8}$$

$$N_\theta = \frac{E\alpha H}{r^2}\left(\frac{r^2}{b^2}\int_0^b r\overline{T}(r)\,dr + \int_0^r r\overline{T}(r)\,dr - r^2\overline{T}(r)\right).$$

Integration of these equations using Eqn. (3) leads to the stresses:

$$\sigma_{rr} = \left[\frac{E\alpha(T_{\max} - T_0)}{8}\right]\left[\left(\frac{a}{b}\right)^2\left(1 - e^{-2b^2/a^2}\right)\right. \tag{9}$$

$$\left. - \left(\frac{a}{r}\right)^2\left(1 - e^{-2r^2/a^2}\right)\right]\left(1 - \frac{2z}{H}\right);$$

$$\sigma_{\theta\theta} = \left[\frac{E\alpha(T_{\max}-T_0)}{8}\right]\left[\left(\frac{a}{b}\right)^2\left(1-e^{-2b^2/a^2}\right) + \left(\frac{a}{r}\right)^2\left(1-e^{-2r^2/a^2}\right) - 4e^{-2r^2/a^2}\right]\left(1-\frac{2z}{H}\right). \tag{10}$$

Fig. 3

The radial stress (Figure 3) has a single compressive extremum at $(r,z) = (0,-H/2)$. The hoop stress has a compressive extremum at $(r,z) = (0,-H/2)$ and a tensile extremum at $(r,z) = (1.2676\,a,-H/2)$; the tensile extremum is located at the edge of the plate ($r = b$) for $a/b > 0.789$. The compressive extremum of hoop stress has a larger magnitude than the tensile extremum if $a/b < 0.96468$; both stresses tend to zero as $a/b \longrightarrow \infty$ (the limit of uniform surface temperature).

Onset of yielding was determined using distortion energy theory (Ugural and Fenster, 1975). To find the flux at onset of yielding, T_{max} was increased until the von Mises stress, $\sigma_v = (\sigma_{rr}^2 - \sigma_{rr}\sigma_{\theta\theta} + \sigma_{\theta\theta}^2)^{1/2}$, exceeded σ_Y at some point in the plate. The yield stress, σ_Y, was evaluated at the local temperature of the plate at the points of maximum stress, while other mechanical properties were evaluated at the thickness-average temperature for $r = 0$.

Table 2

Values of $T_{\max}$ and the heat flux at onset of yielding are given in Table 2. (Data have been omitted from the table where temperatures exceeded the range in which reliable property data were available.) Note that the stresses depend on the temperature difference, rather than the heat flux, so that plates of different thickness will reach yielding for the same value of $T_{\max}$ but with different values of the flux. The numerical values of $q \cdot H$ in the table correspond to the flux at $r = 0$ through a 1 mm plate; for other thicknesses, the flux can be found by dividing the tabulated value by H in millimeters. For example, with $a/b = 0.1$, a DS copper plate of 1 mm thickness yields at a heat flux of 112 MW/m^2 at the plate center, while a 3 mm thick plate will yield at a flux of 37 MW/m^2. The total power of the gaussian source (from $r = 0$ to ∞) is $q(\pi a^2/2)$ at yielding.

In the uniform temperature limit ($a/b \longrightarrow \infty$), where theoretical stresses are zero, the melting point temperature and flux are given. For real plates, this flux is optimistic, in so far as variations of thermal conductivity over these large temperature ranges can be expected to produce nonlinearities in the temperature distributions which will cause significant thermal stresses.

Hardened copper alloys show the highest flux among these materials prior to yielding. Tungsten behaves as both a brittle and ductile material in this configuration (in the cold and hot regions, respectively); thus, its failure point is determined by comparing its stress field to both the ultimate and yield strengths. Aluminum loses strength quickly with increasing temperature, and does not perform well in spite of its high conductivity. Tungsten and molybdenum require protection from oxidation for service temperatures above 770 K.

3.2 Fixed-edge Plate

Here, the edge has zero vertical or radial deflection and zero slope. The solutions for the bending moments are (Goodier, 1957)

$$\begin{aligned} M_r &= \frac{EH^2}{12}\left[\frac{1}{r^2}F(r) + \left(\frac{1+\nu}{1-\nu}\right)\frac{1}{b^2}F(b)\right] \\ M_\theta &= \frac{EH^2}{12}\left[\alpha\Delta T(r) - \frac{1}{r^2}F(r) + \left(\frac{1+\nu}{1-\nu}\right)\frac{1}{b^2}F(b)\right]. \end{aligned} \tag{11}$$

The membrane forces are (Napolitano, 1995)

$$\begin{aligned} N_r &= -\frac{E\alpha H}{r^2}\left[\frac{r^2}{b^2}\left(\frac{1+\nu}{1-\nu}\right)\int_0^b r\overline{T}(r)\,dr + \int_0^r r\overline{T}(r)\,dr\right] \\ N_\theta &= -\frac{E\alpha H}{r^2}\left[\frac{r^2}{b^2}\left(\frac{1+\nu}{1-\nu}\right)\int_0^b r\overline{T}(r)\,dr - \int_0^r r\overline{T}(r)\,dr + r^2\overline{T}(r)\right]. \end{aligned} \tag{12}$$

Integration of these equations using Eqn. (3) provides the stresses:

$$\begin{aligned} \sigma_{rr} = -\left[\frac{E\alpha(T_{\max}-T_0)}{8}\right]\Bigg[&\left(\frac{a}{r}\right)^2\left(1-e^{-2r^2/a^2}\right) \\ &+\left(\frac{1+\nu}{1-\nu}\right)\left(\frac{a}{b}\right)^2\left(1-e^{-2b^2/a^2}\right)\Bigg]\left(1-\frac{2z}{H}\right); \end{aligned} \tag{13}$$

$$\begin{aligned} \sigma_{\theta\theta} = -\left[\frac{E\alpha(T_{\max}-T_0)}{8}\right]\Bigg[&\left(\frac{1+\nu}{1-\nu}\right)\left(\frac{a}{b}\right)^2\left(1-e^{-2b^2/a^2}\right) \\ &-\left(\frac{a}{r}\right)^2\left(1-e^{-2r^2/a^2}\right)+4e^{-2r^2/a^2}\Bigg]\left(1-\frac{2z}{H}\right). \end{aligned} \tag{14}$$

The radial stress has a single compressive extremum at $(r,z) = (0,-H/2)$ (Figure 4). The hoop stress has a compressive extremum at $(r,z) = (0,-H/2)$ and a tensile extremum at $(r,z) = (1.2676\,a,-H/2)$. The compressive extremum of hoop stress has a larger magnitude than the tensile extremum; the tensile extremum becomes a compressive extremum for $a/b > 0.485$ (with $\nu = 0.3$) and is located at the edge of the plate ($r = b$) for $a/b > 0.789$.

Fig. 4

Values of $T_{\max}$ and the heat flux at the onset of yielding are given in Table 3. When $a/b \ll 1$ (a localized hot-spot), the results are identical to those for a simply supported plate: edge constraints are unimportant in this limit. For larger a/b, the heat fluxes at onset of yielding are considerably lower for a fixed plate than for a simply supported plate, owing to higher compressive membrane stresses. One consequence is that allowable temperatures prior to yielding are much lower. As a result, materials with poor

high temperature strength, like aluminum, perform somewhat less poorly relative to
Table 3 other materials.

The solution for uniform heating can be obtained from Eqns. (13–14) by letting $a/b \longrightarrow \infty$. The results are generally well-known (Johns, 1965) and contain both membrane stress and bending stress:

$$\sigma_{rr} = \sigma_{\theta\theta} = -\left[\frac{E\alpha(T_{\max} - T_0)}{2(1-\nu)}\right]\left(1 - \frac{2z}{H}\right). \tag{15}$$

The maximum stresses are compressive and occur on the hot surface ($z = -H/2$); the stress at the opposite surface is zero. In this situation, both temperature and stress are independent of radius. The uniformly-heated fixed-edge limit is the most unfavorable situation for thermal stress. To reach higher fluxes without yielding in a uniform heating configuration, the heat transfer surface should be designed to allow lateral expansion that relieves the membrane stresses.

Restrictions

Cooling system pressure will add additional stress within the plate which may either exacerbate or ameliorate the thermal stress. Such stresses should be compared to thermal stresses in any effort to design with the present results (see, *e.g.*, Lienhard et al., 1996). Generally, pressure stresses will be proportional to $p(b/H)^2$, for p the gage pressure, so that these stresses are most significant for high aspect ratio plates.

The solutions given above are based on classical plate theory, which is valid only when the membrane stresses do not contribute to the bending deflection and when nonlinear strains can be neglected. These conditions are generally met when the plate deflection w is small compared to the plate thickness H. Since the size of the deflection increases with plate diameter, this implies that our solutions are valid only for sufficiently small values of b/H.

The limiting value of b/H can be estimated by finding the value of $\zeta = (1+\nu)\alpha\Delta T(b/H)^2$ below which either the nonlinear strains can be ignored (roughly $w/H < 0.1$) or the error in the classical solution for w is less than 10% (the contribution of bending deflection to the stress is order of unity for all cases other than the fixed-edge case with $a/b \longrightarrow \infty$). The error in the fixed-edge solution has been estimated using Pal's
Table 4 finite amplitude equations (Pal, 1969) for $a/b \geq 0.7$

The limiting value of ζ is given for each case in Table 4. For all simply supported cases and the fixed-edge case with $a/b = 0.1$ and 0.4, the limiting values are those at which the classical plate solution for w/H (Goodier, 1597) reaches 10%. For the other fixed-edge cases, the values are those at which the classical deflection differs from Pal's solution by 10%; when $a/b \longrightarrow \infty$, the fixed-edge limit is that for buckling of the plate.

As an example, a fixed-edge TZM plate with $a/b = 0.75$ will be described by our solutions while $\zeta \leq 0.85$ or, with $\alpha\Delta T$ calculated from data in Tables 1 and 3, for $b/H \leq 15$ — plates whose diameters are no more than 30 times their thickness. For a DS copper plate under the same conditions, the diameter should not exceed 26 times the thickness.

Acknowledgements

JHL was funded by the INEEL University Research Consortium. The INEEL is managed by Lockheed Martin Idaho Technologies Company for the U.S. Department of Energy, Idaho Operations Office under Contract No. DE-AC07-94ID13223. DSN was supported by a fellowship from the Defense Nuclear Facilities Safety Board.

References

M.A. Abdou *et al.*, 1984, "Technical Assessment of the Critical Issues and Problem Areas in High Heat Flux Materials & Component Development," Vol. 2 of "Magnetic Fusion Energy Plasma Interactive and High Heat Flux Components," DOE Office of Fusion Energy Task Group on High Heat Flux Material and Component Development. Los Angeles: Center for Plasma Physics and Fusion Engr., UCLA.

ASM, 1985, *Metals Handbook*, 9th ed. Metals Park, OH: American Society for Metals.

B.A. Boley and J.E. Weiner, 1960, *Theory of Thermal Stresses*. John Wiley: New York.

R.S. Dahbura, 1996, personal communication, MIT, Cambridge MA.

J.N. Goodier, 1957, "Thermal Stress and Deformation," *J. Applied Mech.*, September, pp.467-474.

J.M. Holt, H. Mindlin, and C.Y. Ho (ed.), 1995, *Structural Alloys Handbook*. West Lafayette: CINDAS, Purdue University.

D.J. Johns, 1965, *Thermal Stress Analyses*. Oxford: Pergamon Press.

J.H. Lienhard V, R.S. Dahbura, H.F. Younis, and C.H. Oh, 1996, "Large Area Jet-Array Cooling Modules for High Heat Fluxes," *High Heat Flux Engineering III*. Bellingham, WA: Society of PhotoOptical Instrumentation Engineers, SPIE Vol. 2855, pp.66–81.

J.H. Lienhard V and A.M. Khounsary, 1993, "Liquid Jet Impingement Cooling in Conjunction with Diamond Substrates for Extremely High Heat Flux Applications," *High Heat Flux Engineering II*. Bellingham, WA: Society of PhotoOptical Instrumentation Engineers, SPIE Vol. 1997, pp.29–43.

J.H. Lienhard V and D.S. Napolitano, 1996, "Thermal Stress Limits of Plates Subjected to Extremely High Heat Flux," *Proc. Heat Transfer Division Vol. 2*, ASME HTD-

Vol. 333, pp.23–35.

X. Liu and J.H. Lienhard V, 1993, "Extremely High Heat Fluxes Beneath Impinging Liquid Jets," *J. Heat Transfer*, Vol. 115, pp.472–476.

D.S. Napolitano, 1995, "Stress Induced Failure in Materials Subjected to Extremal Heat Fluxes," S.M. Thesis in Mechanical Engineering, MIT, Cambridge, MA.

M.C. Pal, 1969, "Large Deflections of Heated Circular Plates," *Acta Mechanica*, Vol. 8, pp. 82-103.

D. Peckner and I.M. Bernstein (ed.), 1977, *Handbook of Stainless Steels*. New York: McGraw-Hill.

T.R. Tauchert, 1986, "Thermal Stresses in Plates — Statical Problems," in *Thermal Stresses*, R.B. Hetnarski, ed., Vol. 1. New York: Elsevier Science Publishers.

T.E. Tietz and J.W. Wilson, 1965, *Behavior and Properties of Refractory Metals*. Stanford, CA: Stanford University Press.

Y.S. Touloukian, 1979, *Thermophysical Properties of Matter*, Vol. 1. West Lafayette: Purdue University.

A.C. Ugural and S.K. Fenster, 1975, *Advanced Strength and Applied Elasticity*. New York: Elsevier.

List of Tables

List of Figures

Table 1: Thermal and elastic properties of various materials at room temperature (unless otherwise indicated). Properties that have been estimated are italicized. Units are as follow: α, 10^{-6} K^{-1}; E, GPa; k, W/m·K; σ_Y, MPa; Q_{efm}, MW·mm/m^2; $\Delta T = Q_{\mathrm{efm}}/k$, K; T_{melt}, K. σ_Y for ductile materials is for 0.2% offset. For brittle materials, σ_Y is the compressive strength. T_{melt} is the solidus temperature for metallic alloys; for diamond, it is the temperature above which pyrolysis occurs. α is based on total expansion from 20°C to the indicated temperature.

Material	α	E	k	σ_Y	ν	Q_{efm}	ΔT	T_{melt}
Diamond (single crystal)	0.8	1050	2100	3000	0.15	6400	3	973
DS Copper (C15715-H04)								1356
20°C	*16*	130	365	430	*0.3*	52.8	145	
200°C	17.2	*120*	345	375	*0.3*	43.9	127	
400°C	18.8	*110*	320	307	*0.3*	33.3	104	
Copper-Cr (C18200-TH04)								1343
20°C	16.3	130	324	520	*0.3*	55.6	172	
200°C	17.2	*120*	351	441	*0.3*	55.5	150	
400°C	18.9	109	364	343	*0.3*	42.4	117	
Copper-Zr (C15000-TH04)	16.9	129	367	411	0.34	45.7	124	1253
Molybdenum (TZM)								2883
Stress relieved, 21°C	4.9	315	120	860	*0.3*	46.8	390	
Stress relieved, 1090°C	5.6	205	100	435	*0.3*	26.5	265	
Tantalum (T-222)								3293
Stress relieved, 20°C	5.9	200	54	950	*0.3*	30.4	563	
Stress relieved, 1000°C	6.8	*140*	59	700	*0.3*	30.3	514	
Tungsten								3683
Wrought, 200°C	4.3	400	150	640	0.28	40.0	267	
Wrought, 500°C	4.4	388	130	517	0.29	28.0	215	
Wrought, 1000°C	4.7	367	110	413	0.29	18.4	168	
Recrystallized, 200°C	4.3	400	150	405	0.28	25.3	169	
Recrystallized, 500°C	4.4	388	130	131	0.29	7.1	54	
Niobium (FS-85)								2741
Stress relieved, 20°C	7.1	140	45	735	*0.3*	23.3	518	
Stress relieved, 500°C	7.4	130	49	560	*0.3*	20.0	407	
Recrystalized, 1090°C	9.0	125	57	200	*0.3*	7.1	124	
Aluminum (6061-T651)								855
20°C	23.6	70	167	276	0.33	18.8	112	
149°C	24.2	64	175	215	*0.33*	16.8	96	
371°C	25.3	39	181	12	*0.33*	1.5	9	
Vanadium (V-15Cr-5Ti)	9	124	24	500	*0.3*	10.8	448	2173
Inconel 713C	10.6	205	11	740	*0.3*	2.6	238	1533
Stainless 304L (10% cw)	17.3	193	15	450	*0.27*	1.5	98	1673

Table 2: Temperature and heat flux at which a simply supported plate reaches yield stress during localized heating: $T_{\max}$ in kelvin and $q \cdot H$ in MW·mm/m^2.

Material		a/b				
		0.1	0.4	0.75	1.0	∞
DS Copper (C15715-H04)	$T_{\max}$	616	633	696	766	1343
	$q \cdot H$	*112*	*118*	*138*	*160*	*323*
Chromium Copper (C18200-TH04)	$T_{\max}$	641	659	711	765	1343
	$q \cdot H$	*120*	*127*	*146*	*167*	*376*
Tungsten (wrought)	$T_{\max}$	873	907			3683
	$q \cdot H$	*78*	*82*			*376*
Tungsten (recrystallized)	$T_{\max}$	599	610	645	688	3683
	$q \cdot H$	*43*	*45*	*50*	*55*	*340*
Molybdenum (recrystallized)	$T_{\max}$	556	575	630	705	2883
	$q \cdot H$	*35*	*37*	*44*	*53*	*200*
Aluminum (6061-T651)	$T_{\max}$	461	466	477	491	885
	$q \cdot H$	*28*	*29*	*31*	*33*	*106*
Stainless Steel (304L, 10% cw)	$T_{\max}$	502	515	561	615	1670
	$q \cdot H$	*3*	*3*	*4*	*5*	*35*

Table 3: Temperature and heat flux at which a fixed-edge plate reaches yield stress during localized heating: $T_{\max}$ in kelvin and $q \cdot H$ in MW·mm/m^2.

Material		a/b				
		0.1	0.4	0.75	1.0	∞
DS Copper (C15715-H04)	$T_{\max}$	610	581	525	494	429
	$q \cdot H$	*110*	*100*	*82*	*71*	*49*
Chromium Copper (C18200-TH04)	$T_{\max}$	639	610	555	523	450
	$q \cdot H$	*119*	*109*	*89*	*77*	*52*
TZM Alloy (wrought)	$T_{\max}$	1052	980	841	764	606
	$q \cdot H$	*94*	*86*	*70*	*60*	*41*
Tungsten (wrought)	$T_{\max}$	864	811	714	643	557
	$q \cdot H$	*77*	*71*	*59*	*49*	*38*
Tungsten (recrystallized)	$T_{\max}$	598	579	543	522	473
	$q \cdot H$	*43*	*41*	*36*	*33*	*26*
Molybdenum (recrystallized)	$T_{\max}$	556	525	478	450	395
	$q \cdot H$	*35*	*31*	*24*	*21*	*13*
Aluminum (6061-T651)	$T_{\max}$	461	455	442	430	400
	$q \cdot H$	*28*	*27*	*25*	*23*	*17*
Stainless Steel (304L, 10% cw)	$T_{\max}$	502	478	438	420	381
	$q \cdot H$	*3*	*3*	*2*	*2*	*1*

Table 4: Values of $\zeta = (1 + \nu)\alpha\Delta T(b/H)^2$ below which classical plate results are applicable.

Boundary Condition	a/b				
	0.1	0.4	0.75	1.0	∞
Fixed edge	16.4	2.4	0.85	0.50	2.4
Simply supported	12.5	1.4	0.60	0.45	0.26

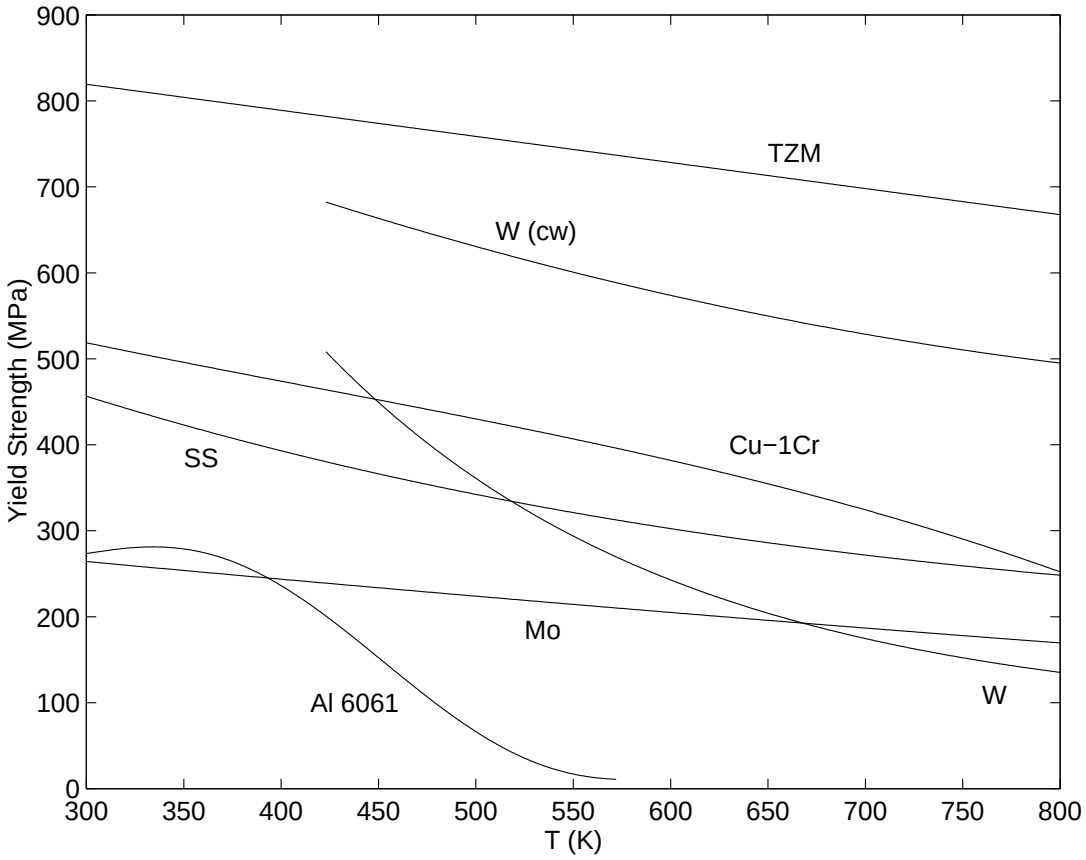

Figure 1: Temperature dependence of 0.2% yield stress σ_Y for various metals: aluminum (6061-T651), molybenum (recrystalized), tungsten (recrystalized), 304L stainless steel (10% cold work), chromium copper (18200-TH04), tungsten (wrought), TZM (stress-relieved)

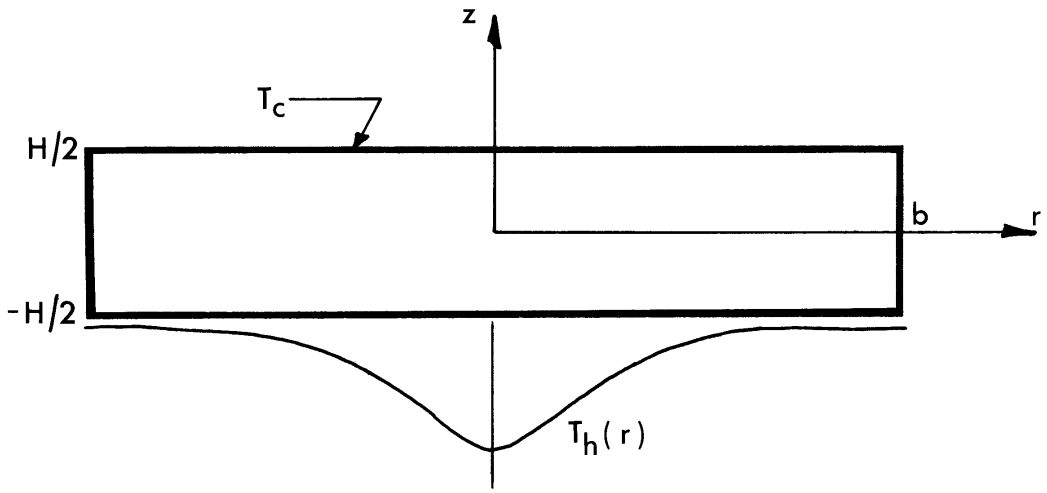

Figure 2: A circular disc subjected to a Gaussian temperature distribution on one surface.

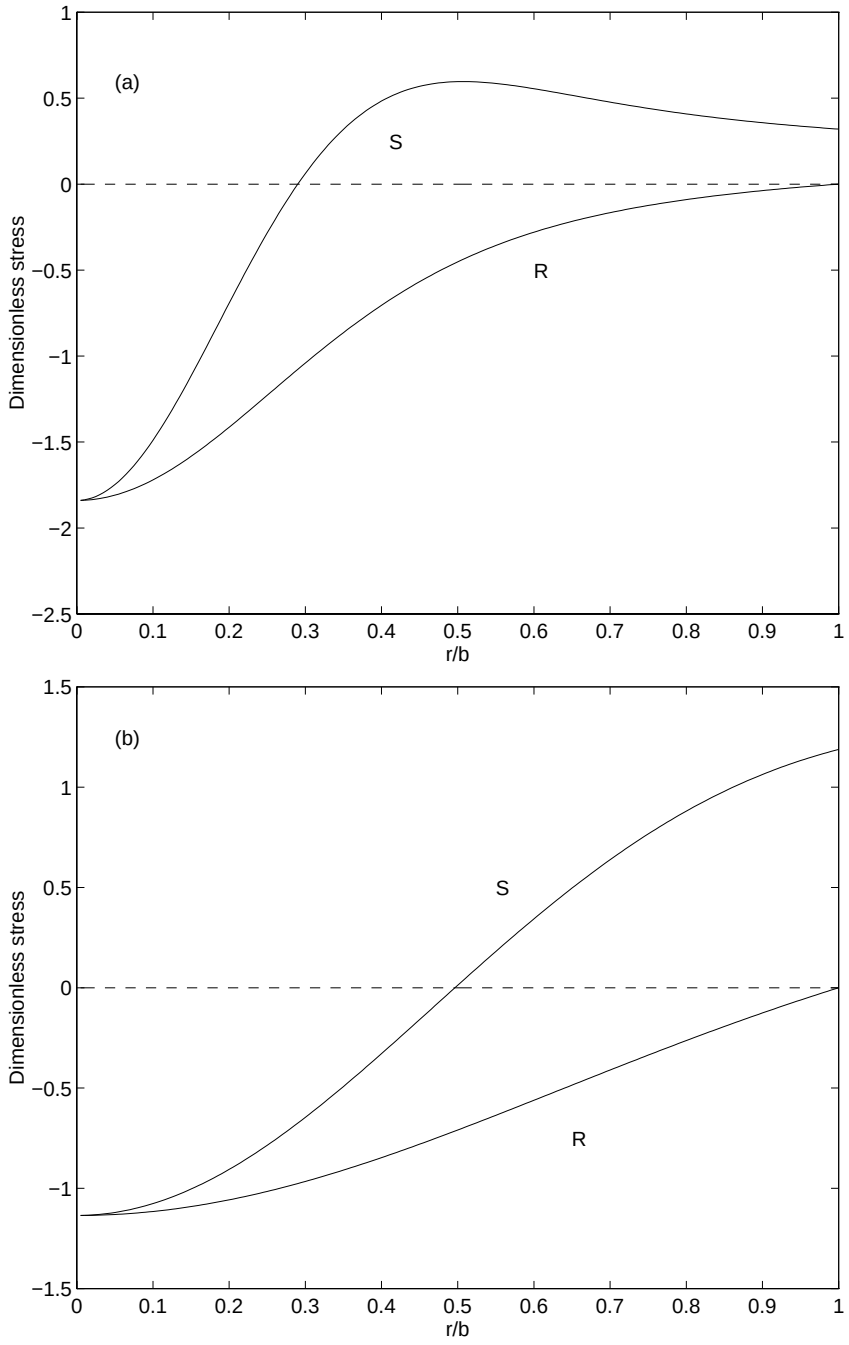

Figure 3: Normalized distributions of σ_{rr} and $\sigma_{\theta\theta}$ at $z = -H/2$ in a simply supported circular disk: (a) $a/b = 0.4$, (b) $a/b = 1.0$. $R = 4\sigma_{rr}/[E\alpha(T_{\max} - T_0)]$, $S = 4\sigma_{\theta\theta}/[E\alpha(T_{\max} - T_0)]$.

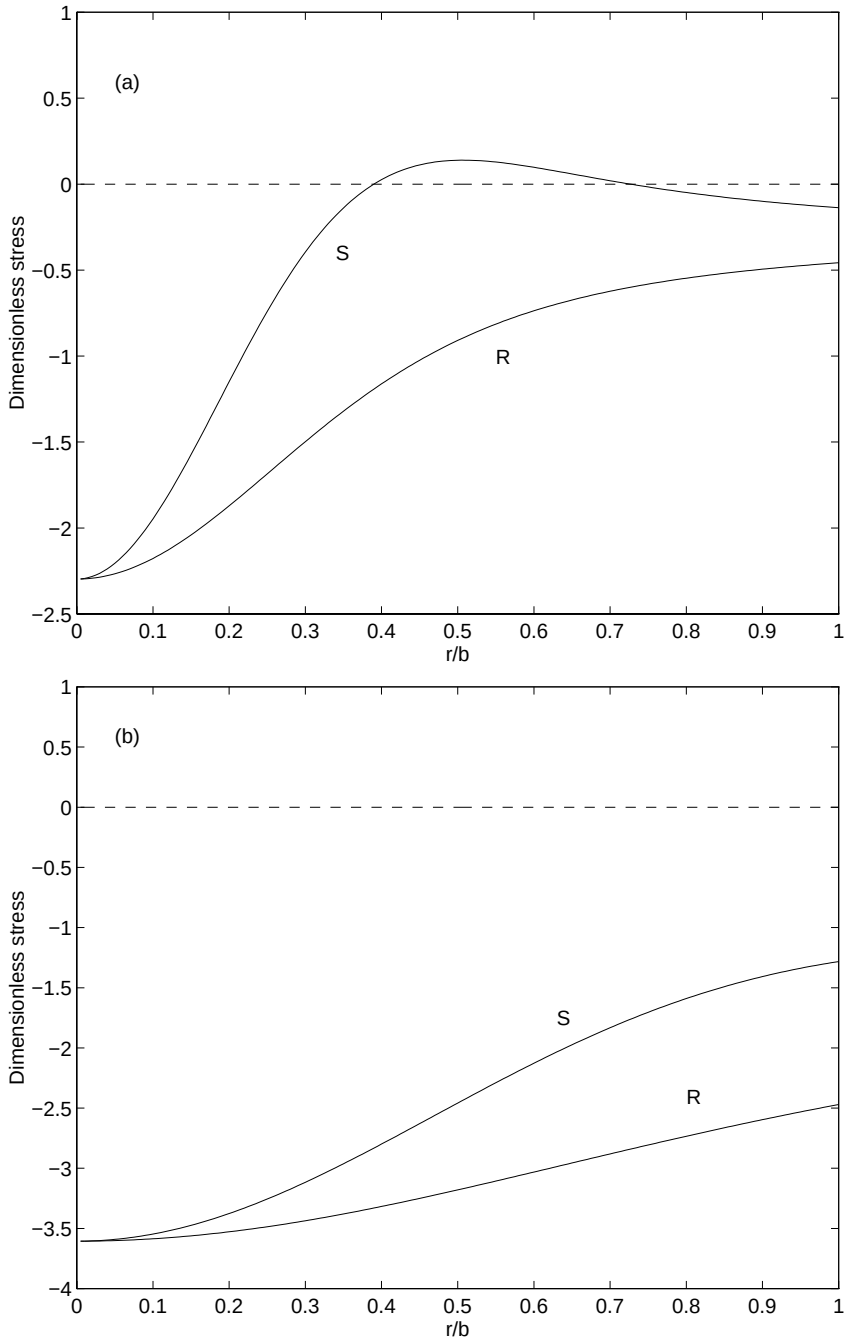

Figure 4: Normalized distributions of σ_{rr} and $\sigma_{\theta\theta}$ at $z = -H/2$ in a circular disk fixed along its outer radius: (a) $a/b = 0.4$, (b) $a/b = 1.0$. $R = 4\sigma_{rr}/[E\alpha(T_{\max} - T_0)]$, $S = 4\sigma_{\theta\theta}/[E\alpha(T_{\max} - T_0)]$.